

Functional group resolved nuclear spin relaxation in porous media

Neil Robinson, Eric F. May and Michael L. Johns*

Department of Chemical Engineering, University of Western Australia, 35 Stirling Highway, Perth, WA 6009, Australia

***Corresponding Author:**

Prof Mike Johns
Chair of Chemical and Process Engineering
University of Western Australia

Postal Address:

Department of Chemical Engineering
The University of Western Australia
35 Stirling Highway (M050)
Perth WA 6009
Australia

Phone: +61 (08) 6488 5664

Email: michael.johns@uwa.edu.au

Fluid Science and Resources Research Group: www.fsr.ecm.uwa.edu.au

Author ORCID:

Neil Robinson	0000-0002-0893-2190
Eric F. May	0000-0001-5472-6921
Michael L. Johns	0000-0001-7953-0597

1 **Abstract**

2 Understanding solid-fluid interactions within porous materials is critical for their efficient utilisation across
3 chemical reaction and separation processes. However, detailed characterisation of interfacial phenomena
4 within such systems is hampered by their optically opaque nature. Motivated by the need to bridge this
5 capability gap, we detail here the application of low magnetic field 2D ^1H nuclear spin relaxation
6 measurements as a non-invasive probe of sorbate/sorbent interactions, exploring the relaxation
7 characteristics exhibited by liquid adsorbates confined to a model mesoporous silica. For the first time, we
8 demonstrate the capacity of such measurements to distinguish functional group-specific relaxation
9 phenomena across a diverse range of protic adsorbates of wide importance as solvents, reagents, and
10 hydrogen carriers, with distinct relaxation environments assigned to the alkyl and hydroxyl moieties of the
11 confined liquids. Uniquely, this relaxation behaviour is shown to correlate with adsorbate acidity, with the
12 observed relationship rationalised on the basis of surface-adsorbate proton exchange dynamics.

1 Introduction

2 Characterisation of the solid-liquid interface is critical for the rational development of technologies across the
3 medical, corrosion, environmental and energy sciences.¹ However, spectroscopic interrogation of the chemical
4 and physical nature of such interfaces remains severely impeded by the need to differentiate the species of
5 interest from the surrounding solid and liquid components. In the case of porous solids – essential to diverse
6 industrial processes such as separations, catalysis, and energy storage – straightforward characterisation of
7 interfacial phenomena is further hindered by the heterogeneous and optically opaque nature of the materials
8 employed, which in turn preclude spectroscopic approaches which necessitate unimpeded access to well-
9 defined surfaces, or require thin adsorbate films.²

10 Nuclear spin relaxation measurements have emerged as a versatile, chemically selective, and non-invasive
11 route for the characterisation of such systems.^{3,4} Utilising appropriate nuclear magnetic resonance (NMR)
12 pulse sequences and hardware this experimental approach measures the longitudinal and/or transverse
13 relaxation behaviour of the spin system under study, as characterised by the time constants T_1 and T_2 ,
14 respectively. While these time constants conform to well-defined relationships with the translational and
15 rotational dynamics of spin-bearing molecules in the unrestricted bulk liquid phase,⁵ the restricted dynamics
16 of fluids within porous media often results in complex relaxation behaviour associated with surface
17 interactions and confinement effects, providing potential insight into both material characteristics and
18 interfacial phenomena.⁶ Such measurements have been employed by the rock physics and petrochemical
19 exploration communities for over five decades,^{7,8} providing estimates of oil and gas reservoir quality indicators
20 including pore size distributions, porosity, permeability, and producible hydrocarbon content.⁹ Further well-
21 established applications include the observation of cement and plaster hydration kinetics,^{10,11} while emergent
22 fields within the materials chemistry research space now include characterisation of bespoke porous
23 architectures including heterogeneous catalysts,^{12–14} zeolites¹⁵ and metal-organic frameworks.¹⁶

24 The most data-rich methods for elucidating spin relaxation processes in porous media are multidimensional
25 relaxation correlation measurements.^{17–19} Indeed, two-dimensional (2D) relaxation-relaxation ($T_1 - T_2$ ^{20–22}
26 and $T_2 - T_2$ ^{23,24}) and diffusion-relaxation ($D - T_2$ ^{25–28}) measurements are widely applied to characterise the
27 dynamics of confined fluids, while higher-dimensional experiments,^{29–32} including variants exhibiting spatial
28 resolution,^{33,34} have also been reported. Such measurements are of particular utility in the study of fluids
29 confined to heterogeneous solids as they are essentially independent of the detailed chemical shift
30 phenomena associated with traditional frequency-based NMR methods, wherein spectral peaks are likely to
31 be (i) dominated by species away from the interface of interest, and (ii) unfavourably broadened due to the
32 effects of magnetic susceptibility differences at the solid-liquid interface,³⁵ often requiring exotic approaches
33 (see e.g. ref³⁶) to avoid an intractable loss of spectral resolution.

1 Here we focus on the interpretation of 2D ^1H (proton) $T_1 - T_2$ relaxation correlation data as a probe of
2 adsorbate identity and interfacial dynamics. Such measurements are particularly advantageous in the
3 presence of multiple fluids, with differences in observed relaxation times – often by an order of magnitude or
4 more – facilitating distinction between components. An established example of this phenomenon is the
5 characterisation of hydrocarbon-bearing shale rocks,^{37,38} wherein the contributions of oil, gas and bituminous
6 hydrocarbons are often readily identified. As first demonstrated by Weber *et al.*,³⁹ this concept is also
7 extensible to the observation of competitive displacement processes, wherein the relative populations of
8 correlation peaks associated with different liquids may be followed simultaneously to provide insight into
9 displacement kinetics.

10 In this work, the concept that multiple fluids within the same porous material can present distinct relaxation
11 correlation populations is extended to the realisation and interpretation of relaxation data associated with a
12 single probe fluid exhibiting multiple observable nuclear spin relaxation environments. Specifically, through
13 the exploitation of a series of short-chain alcohols and carboxylic acids imbibed within a model mesoporous
14 silica, we demonstrate for the first time that a wide range of polar-protic adsorbates exhibit discrete proton
15 relaxation characteristics associated with their different hydrogen-bearing moieties. We find that such
16 observations facilitate clear spectroscopic distinction between alkyl and hydroxyl groups without the need for
17 chemical shift analysis. Further motivated by the discovery of a correlation between relaxation characteristics
18 and adsorbate acidity, we provide a clear rationalisation for the observed functional group-specific surface
19 relaxation phenomena in terms of interfacial proton exchange dynamics.

20

1 Results

2 Nuclear spin relaxation of confined liquids

3 **Figure 1** summarises our experimental approach: Measurements utilised a 2D $T_1 - T_2$ correlation pulse
4 sequence (**Figure 1a**) implemented on a 12.7 MHz benchtop NMR spectrometer (**Figure 1b**). Samples
5 comprised a range of short chain liquid hydrocarbons imbibed within a particulate silica material (4 mm
6 diameter particles) exhibiting 15 nm pores (**Figure 1c**); mesoporous silica was selected as a model porous solid
7 in this work due to its wide-ranging application as a support material in heterogeneous catalysis, and hence
8 relevance to a plethora of interfacial processes.⁴⁰ Further experimental details are provided in **Methods**.

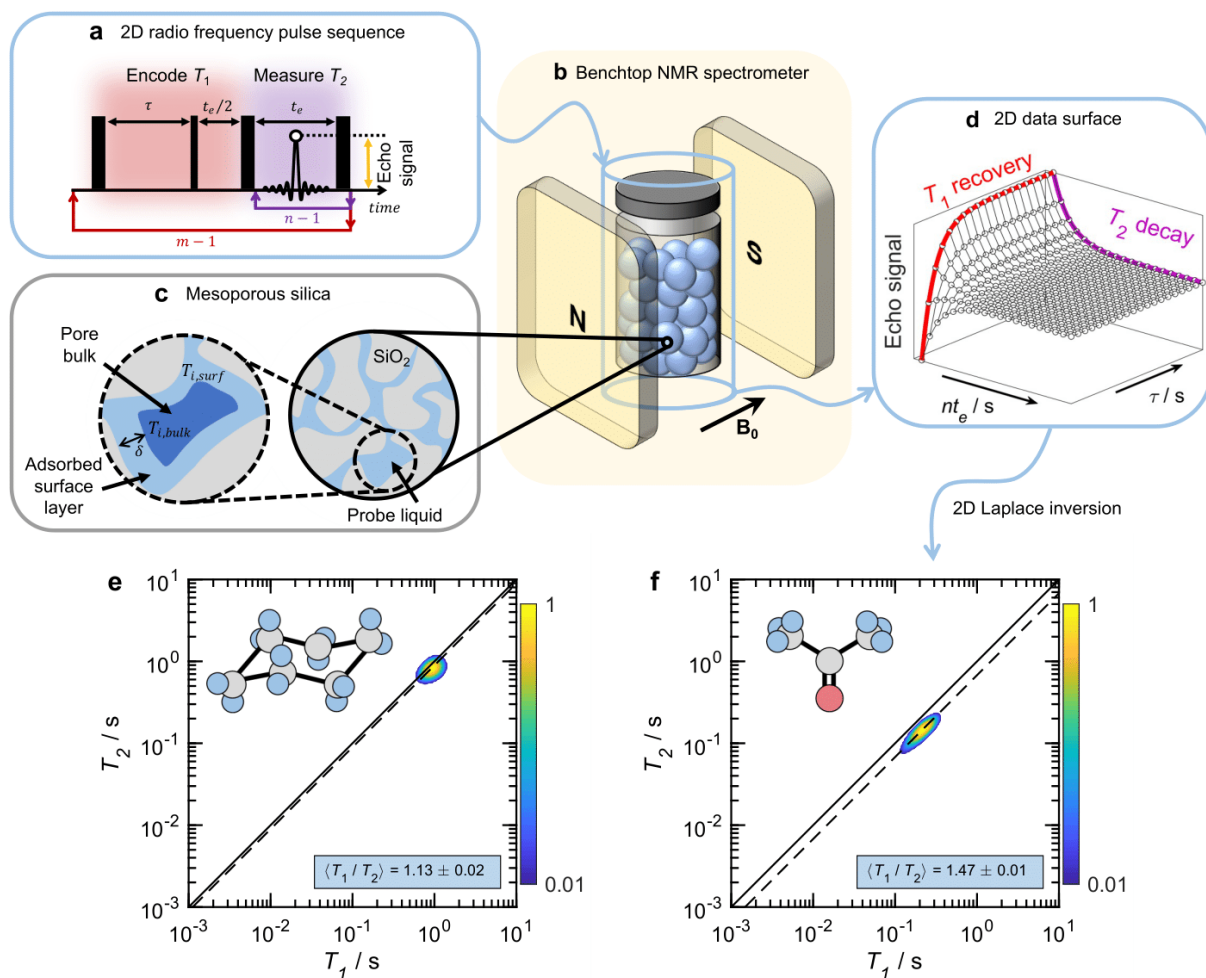
9 The $T_1 - T_2$ correlation experiment employed here measures a series of T_2 relaxation decay processes
10 exhibiting differing degrees of T_1 encoding (**Figure 1d**). The resulting 2D relaxation data may then be inverted⁴¹
11 to provide a 2D $T_1 - T_2$ population distribution, wherein correlation peaks provide insight into the relative
12 probability of the system exhibiting a given combination of T_1 and T_2 relaxation times. **Figures 1e and 1f** show
13 example correlation data for imbibed cyclohexane and acetone, explored here as archetypal apolar and polar-
14 aprotic adsorbates, respectively. Any liquid outside of the porous material was removed before analysis (see
15 **Methods**) such that all observed relaxation characteristics are associated with confined species. A single
16 correlation peak is observed in each case, characteristic of imbibed species exhibiting a single effective ^1H
17 relaxation environment as a result of fast-exchange between adsorbed species and bulk-like molecules away
18 from the solid-liquid interface.^{42,43} Under such conditions, and assuming surface-limited relaxation,⁶ a well-
19 established general expression for the observed relaxation rates $T_{i,obs}^{-1}$ (with $i \in \{1,2\}$) is known:¹⁷

$$\frac{1}{T_{i,obs}} \approx \frac{1}{T_{i,bulk}} + \frac{S}{V} \frac{\delta}{T_{i,surf}}. \quad (1)$$

20 Here S/V is the surface-to-volume ratio of the confining pore structure, δ the length scale of the adsorbed
21 surface layer, $T_{i,surf}$ the relaxation time constants of the adsorbed population, and $T_{i,bulk}$ the time constants
22 of the unrestricted fluid (see **Figure 1c**). This expression exemplifies the inherent sensitivity of nuclear spin
23 relaxation measurements to both material properties (S/V ; providing sensitivity to pore size) and interfacial
24 chemistry ($\delta/T_{i,surf}$; commonly termed the surface relaxivity). Moreover, given the general case that
25 $T_{i,surf} \ll T_{i,bulk}$, the dimensionless ratio of observed relaxation time constants can be reduced to to
26 $T_{1,obs}/T_{2,obs} \sim T_{1,surf}/T_{2,surf}$.⁴⁴ This surface ratio $T_{1,surf}/T_{2,surf}$ is sensitive to the activated translational
27 dynamics of molecules at the solid-liquid interface,⁴⁵ and is considered a non-invasive probe of surface
28 affinity^{21,46} (additional surface relaxation theory is detailed in **Supplementary Note 1**). As the experimentally
29 accessible ratio $T_{1,obs}/T_{2,obs}$ is largely unaffected by the terms δ and S/V in **Equation (1)**, acquisition of this
30 metric provides a novel route for the comparison of interfacial phenomena either between different porous

1 media imbibed with the same liquid, or as demonstrated here, multiple liquids within the same porous
2 material.

3 As the ill-posed nature of the inversion process required to obtain the 2D relaxation distributions (an inverse
4 Laplace transform⁴⁷) is highly susceptible to the influence of experimental noise,⁴¹ we restrict our analysis of
5 such distributions to the modal relaxation characteristics of each correlation peak observed, making no
6 attempt to infer insight from correlation peak shapes. The modal $T_{1,obs}/T_{2,obs}$ ratios of the correlation peak
7 within **Figures 1e and 1f** (from here on in referred to as $\langle T_1/T_2 \rangle$) are indicated by a dashed diagonal lines, with
8 the larger $\langle T_1/T_2 \rangle$ value of acetone ($\langle T_1/T_2 \rangle = 1.47 \pm 0.01$), compared to cyclohexane ($\langle T_1/T_2 \rangle = 1.13 \pm$
9 0.02) providing a clear demonstration of the increased affinity of polar adsorbates for oxide pore surfaces,
10 relative to apolar alkanes.⁴⁸



1

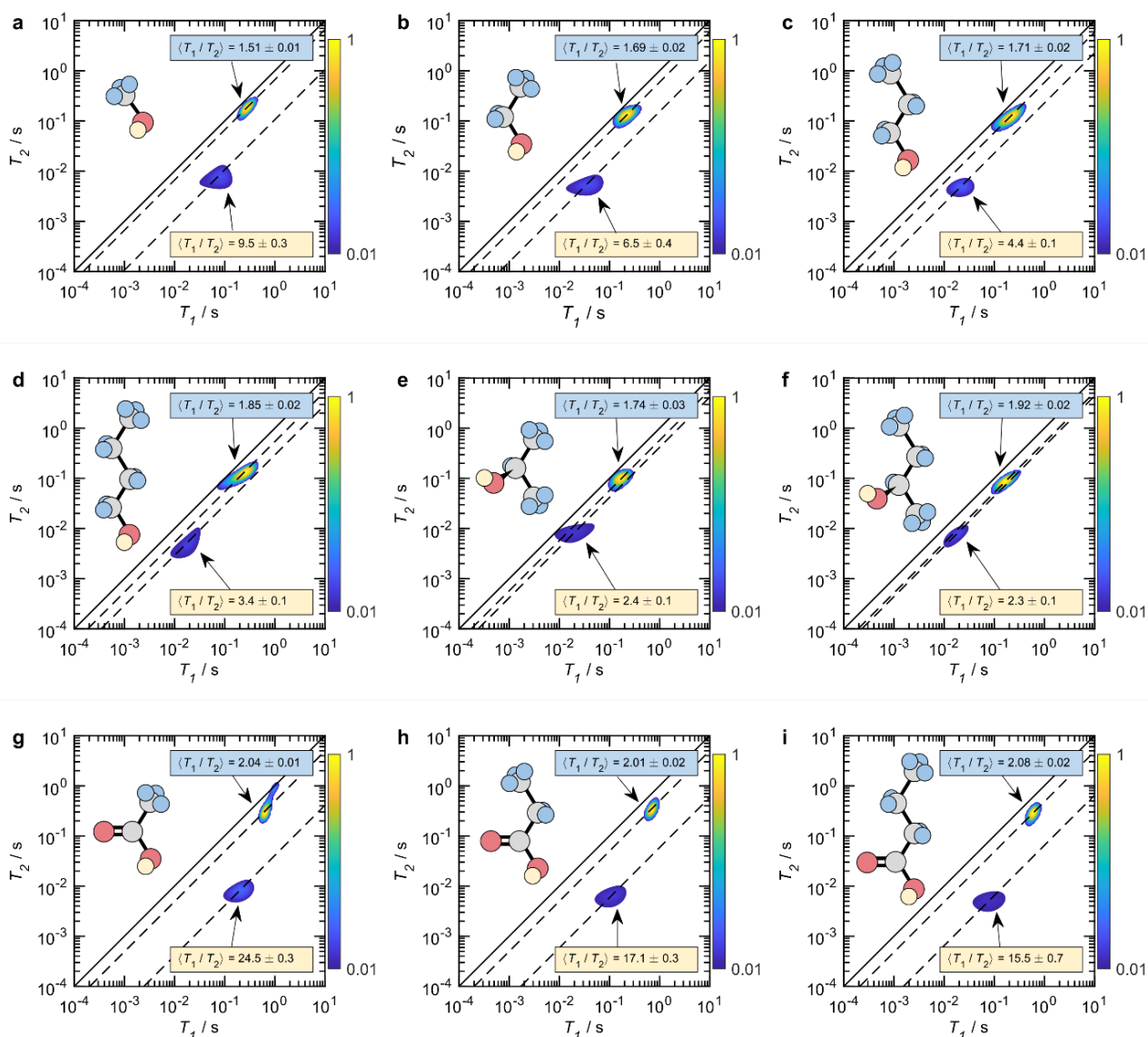
2 **Figure 1. Experimental approach.** Measurements employed (a) a 2D $T_1 - T_2$ pulse sequence and (b) a low-
 3 field benchtop NMR spectrometer with a $B_0 = 0.3$ T ($\nu_0\{^1\text{H}\} = 12.7$ MHz) parallel plate magnet array. The porous
 4 silica (SiO_2) material comprised 4 mm diameter spheres with 15 nm pores (b and c), and was soaked in each
 5 probe liquid for 48 hours, with the inter-particle liquid then removed. By cycling the 2D pulse sequence in (a)
 6 through m different τ values and recording the intensity of the resulting n echoes a ($nt_e \times m\tau$) data surface
 7 is generated (d), which may be inverted to generate a 2D probability distribution of T_1 and T_2 times (see
 8 **Methods**). Example ^1H $T_1 - T_2$ correlation data for cyclohexane and acetone within this silica material are
 9 shown in e and f, respectively. The magnitude of each correlation peak indicates the relative probability of
 10 each system exhibiting a particular combination of T_1 and T_2 relaxation times, as indicated by the colour bars.
 11 Solid diagonal lines indicate the parity ratio $T_1/T_2 = 1$, while the modal relaxation time ratio $\langle T_1/T_2 \rangle$ of each
 12 correlation peak is indicated by dashed diagonal lines; $\langle T_1/T_2 \rangle$ values are specified in each case. The molecular
 13 structure of each adsorbate is also given: C, O and H atoms are coloured grey, red and blue, respectively.

1 Relaxation of polar-protic adsorbates

2 **Figure 2** shows $^1\text{H } T_1 - T_2$ distributions for a series of small polar-protic hydrocarbons within the same silica
3 material; the example adsorbates studied here include short-chain primary alcohols (methanol, ethanol, 1-
4 propanol and 1-butanol), secondary alcohols (2-propanol and 2-butanol) and simple carboxylic acids (acetic
5 acid, propanoic acid and butanoic acid). In contrast to **Figure 1**, two distinct correlation peaks are clearly
6 apparent within each data set, exhibiting significantly different modal T_1 and T_2 times ($\langle T_1 \rangle$ and $\langle T_2 \rangle$),
7 respectively; values are provided in **Supplementary Table 1**. Any inter-particle liquid was again removed from
8 these samples, such that all observed relaxation populations must arise from the confined fluids within the
9 silica pore network. We note these peaks cannot be assigned to the presence of multiple pore environments
10 with varying surface-to-volume ratios (see **Equation (1)**), which, given the similar self-diffusion properties of
11 short-chain alcohols and acids to our aprotic adsorbates (demonstrated elsewhere^{49–51}) would also be
12 apparent within the cyclohexane and acetone data in **Figure 1**. Proton-proton scalar coupling artefacts⁵² may
13 also be discounted due to the very short echo time employed in these measurements (see **Methods**). Rather,
14 these populations are assigned to the distinct relaxation characteristics of the alkyl (C_x^1H_y) and hydroxyl ($-\text{O}^1\text{H}$)
15 proton environments of each adsorbate. Our assignments are supported by previous spectrally-resolved (high-
16 field) T_1 measurements of methanol within a range of porous oxide materials,⁵³ which revealed the hydroxyl
17 proton to exhibit distinctly more rapid rates of T_1 relaxation than those within the alkyl environment.
18 Correlation peaks at short $\langle T_1 \rangle$ and $\langle T_2 \rangle$ values are therefore assigned to the hydroxyl ^1H environments of each
19 adsorbate, while peaks at longer relaxation times are assigned to the corresponding alkyl environments. These
20 assignments are further consistent with the integrated peak ratios obtained from each correlation plot, which
21 we expect to reflect the ratio of protons within each chemical environment; these ratios are correlated against
22 the expected alkyl/hydroxyl ratio of each adsorbate in **Figure 3**, demonstrating a strong, positive correlation.
23 Given the complex surface exchange phenomena described and discussed below, however, we note that a 1:1
24 parity between observed and expected alkyl/hydroxyl ratios is not expected for these data.

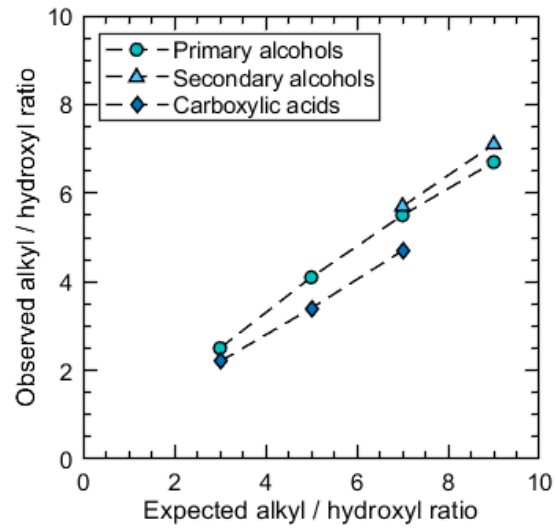
25 While we recognise previous analyses of confined methanol suggest the existence of two distinct relaxation
26 populations,^{21,54–56} the correlation data in **Figure 2** exemplifies the first observation of such phenomena in
27 longer chain primary alcohols, as well as the first such data for both secondary alcohols and carboxylic acids.
28 While high and intermediate field measurements have failed to evidence the existence of multiple relaxation
29 environments in the presence of longer chain ($>\text{C}_1$) liquid hydrocarbons,^{21,56} we attribute the clear and
30 persistent observation of hydroxyl group relaxation phenomena across our range of polar-protic adsorbates
31 to the combination of short experimental echo times and low magnetic field strength (see **Methods**); these
32 experimental conditions significantly reduce the impact of magnetic susceptibility contrast effects on the
33 measurement of short T_2 times,³⁵ facilitating the accurate measurement of relaxation data associated with
34 rapidly relaxing hydroxyl protons. Collectively, the correlation data detailed within **Figure 2** confirms, for the

1 first time, the widespread existence of functional group-specific relaxation phenomena across a broad range
2 of organic molecules of importance as solvents, reagents, and hydrogen carriers. In the remainder of this work
3 we identify and examine distinct trends in the observable relaxation characteristics presented by these
4 adsorbates.



1

2 **Figure 2. Relaxation characteristics of protic adsorbates.** ^1H $T_1 - T_2$ correlation data for **a – d** primary
3 alcohols (**a** methanol, **b** ethanol, **c** 1-propanol and **d** 1-butanol), **e – f** secondary alcohols (**e** 2-propanol and **f**
4 2-butanol), and **g – i** carboxylic acids (**g** acetic acid, **h** propanoic acid and **i** butanoic acid) in mesoporous silica
5 (exhibiting 15 nm pores) at 12.7 MHz. The magnitude of each correlation peak indicates the relative probability
6 of each system exhibiting a particular combination of T_1 and T_2 relaxation times, as indicated by the colour
7 bars. Solid diagonal lines indicate the parity ratio $T_1/T_2 = 1$, while the modal relaxation time ratio $\langle T_1/T_2 \rangle$ of
8 each correlation peak is indicated by dashed diagonal lines; $\langle T_1/T_2 \rangle$ values are specified in each figure. The
9 molecular structure of each adsorbate is also given: C and O atoms are coloured grey and red, respectively.
10 Aprotic H are coloured blue while protic H are shown in yellow. Correlation peaks at long and short T_2 are
11 assigned to aprotic and protic ^1H -containing moieties, respectively.



1

2 **Figure 3. Correlation peak integrals.** Integrated peak ratios from the correlation data presented in Figure 2 as
 3 a function of the expected alkyl/hydroxyl ratio of the same adsorbates.

1 Relaxation, acidity and surface-adsorbate proton exchange

2 **Figure 4a** provides a summary of the $\langle T_1/T_2 \rangle$ values obtained from the correlation data presented in **Figure 2**.
3 A general increase in the alkyl $\langle T_1/T_2 \rangle$ of alcohols is evident with increasing carbon chain length, from
4 $\langle T_1/T_2 \rangle = 1.51 \pm 0.01$ for methanol to $\langle T_1/T_2 \rangle = 1.85 \pm 0.02$ for 1-butanol, and from $\langle T_1/T_2 \rangle = 1.74 \pm$
5 0.08 for 2-propanol to $\langle T_1/T_2 \rangle = 1.92 \pm 0.02$ for 2-butanol. These observations regards the alkyl $\langle T_1/T_2 \rangle$
6 ratio are consistent with previous investigations of short-chain primary alcohol behaviour in porous silica²¹
7 and alumina,⁵⁶ with the measured relaxation time ratios found to correlate with adsorbate surface affinity.²¹
8 Conversely, our hydroxyl $\langle T_1/T_2 \rangle$ values demonstrate a clear decrease with increasing carbon chain length,
9 with this decrease noticeably evident across both the primary alcohol and carboxylic acid data sets. To enable
10 further discussion of this discrepancy we introduce a new metric of the form $\Delta\langle T_1/T_2 \rangle = \langle T_1/T_2 \rangle_{hydroxyl} -$
11 $\langle T_1/T_2 \rangle_{alkyl}$; this metric quantifies the difference in $\langle T_1/T_2 \rangle$ between the alkyl and hydroxyl relaxation
12 populations of each adsorbate and is independent of their absolute values (see **Figure 4a**), which we expect
13 to scale with molecular surface affinity.²¹ The overall progression of $\Delta\langle T_1/T_2 \rangle$ is: carboxylic acids \gg primary
14 alcohols $>$ secondary alcohols (see **Supplementary Table 1** for values), with values further decreasing as a
15 function of increased carbon chain length in each case. Given these behaviours mirror the well-known trends
16 in the acidity of these adsorbates, we conjecture that a comprehensive understanding of our observed
17 relaxation data likely requires consideration of hydroxyl proton dissociation. This interpretation is supported
18 in **Figure 4b** which details a plot of $\Delta\langle T_1/T_2 \rangle$ against adsorbate pK_a , employed here as a convenient metric of
19 liquid-phase acidity. A strong correlation is clearly apparent between increasing $\Delta\langle T_1/T_2 \rangle$ and decreasing pK_a
20 (indicative of increased acidity).

21 We rationalise the above trend through recognition of the dominant surface interaction mechanism between
22 (hydroxylated) silica surfaces and polar protic molecules. Such interactions are governed by surface-adsorbate
23 hydrogen bonding interactions, which provide not only a favourable bonding mode between protic adsorbates
24 and surface-bound hydroxyl groups,^{57,58} but also a well-established means for proton exchange.⁵⁹⁻⁶¹ Exchange
25 interactions during the encoding periods of $T_1 - T_2$ correlation measurements have significant potential to
26 bias the resulting relaxation characteristics. This concept is elucidated by considering two coupled
27 magnetisation reservoirs, M_{sol} and M_{ads} , which we associate with solid-bound and adsorbate-bound hydroxyl
28 protons, respectively. Relaxation during the T_1 and T_2 encoding periods of the pulse sequence in **Figure 1a** is
29 given by:⁶²

$$\frac{d}{dt} \begin{bmatrix} M_{sol} \\ M_{ads} \end{bmatrix} = \begin{bmatrix} -T_{1,sol}^{-1} - k_1 & k_2 \\ k_1 & -T_{1,ads}^{-1} - k_2 \end{bmatrix} \begin{bmatrix} M_{sol} - M_{sol}^0 \\ M_{ads} - M_{ads}^0 \end{bmatrix} \quad (2)$$

30 and

$$\frac{d}{dt} \begin{bmatrix} M_{sol} \\ M_{ads} \end{bmatrix} = \begin{bmatrix} -T_{2,sol}^{-1} - k_1 & k_2 \\ k_1 & -T_{2,ads}^{-1} - k_2 \end{bmatrix} \begin{bmatrix} M_{sol} \\ M_{ads} \end{bmatrix}, \quad (3)$$

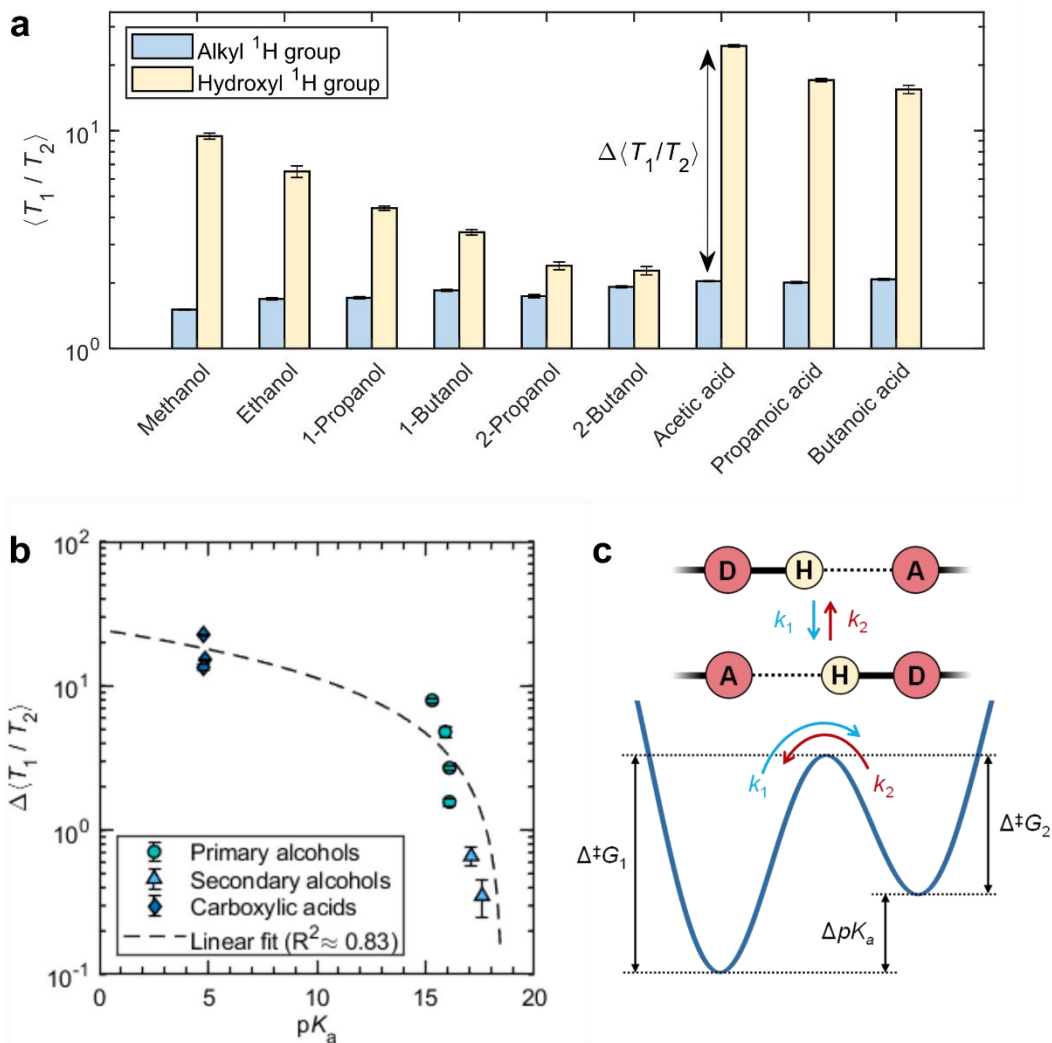
1 respectively, where $T_{i,sol}$ and $T_{i,ads}$ (with $i \in \{1,2\}$) are the relaxation time constants of the two reservoirs.
 2 The terms M_{ads}^0 and M_{sol}^0 are the equilibrium magnetisations of the two reservoirs, which are directly
 3 proportional to the intrinsic number of protons within each environment. The exchange rate constants k_1 and
 4 k_2 then quantify the rates of proton migration between surface and adsorbate hydroxyl groups, with the
 5 overall exchange rate $k = k_1 + k_2$. Simple solutions to these expressions emerge in the limits of and slow
 6 ($k \ll |T_{2,sol}^{-1} - T_{2,ads}^{-1}|$) and fast ($k \gg |T_{1,sol}^{-1} - T_{1,ads}^{-1}|$) exchange, giving rise to either two distinctly separate
 7 relaxation populations or a single, highly averaged population, respectively.⁶³ In the intermediate regime
 8 between these limiting cases the observed relaxation characteristics are sensitive to the relative magnitudes
 9 of the inherent relaxation, exchange rates and equilibrium magnetisations; upon approaching the fast
 10 exchange limit a single population is expected, exhibiting relaxation times sensitive to k .⁶⁴

11 Simple detection of the exchange regime relevant to our data is obviated by the lack of observable surface
 12 hydroxyl populations,^{37,65} with the true relaxation behaviour of our experimental systems further complicated
 13 by adsorption/desorption processes. However, given the high sensitivity of the ratio T_1/T_2 to the adsorbed
 14 surfaced layer (see **Supplementary Note 1**), we conjecture that rapid exchange of this form provides a
 15 significant contribution to the hydroxyl group $\langle T_1/T_2 \rangle$ behaviour observed in **Figure 2**. As solid-state structures
 16 exhibit long T_1 and short T_2 values,⁵ surface-adsorbate proton exchange dynamics occurring near the fast-
 17 exchange limit are expected to decrease the observed hydroxyl T_2 times, while propagating a corresponding
 18 increase in T_1 . An increase in exchange rate is therefore expected to increase $\Delta\langle T_1/T_2 \rangle$ as hydroxyl group
 19 exchange dynamics progressively increase the associated $\langle T_1/T_2 \rangle$ values away from that of the non-
 20 exchanging alkyl environment.

21 Considering the trend demonstrated in **Figure 4b**, the increase in $\Delta\langle T_1/T_2 \rangle$ anticipated to arise from such
 22 dynamics as a function of increased exchange rate clearly suggests that more acidic adsorbates undergo more
 23 rapid rates of proton dissociation at the solid/liquid interface. Despite the typical disparity between the
 24 thermodynamic and kinetic contributions to exchange phenomena, an approximate relationship between
 25 hydroxyl exchange rates and adsorbate acidity is obtained by considering the double-well potential energy
 26 surface in **Figure 4c**. Assuming classical dynamics (i.e. neglecting tunnelling) the exchange rates between free
 27 energy minima is given by the Eyring equation: $k_i = (k_B T/h) \exp(-\Delta^\ddagger G_i/RT)$ (with $i \in \{1,2\}$), where k_B , h
 28 and R are the Boltzmann constant, Planck constant and gas constant, respectively, T is the absolute
 29 temperature, and $\Delta^\ddagger G_i$ are the activation free energy barrier heights. Thermodynamically, the free energy
 30 change for a given proton dissociation process is $\Delta G \approx 2.303RTpK_a$. As proton exchange between potential
 31 wells is considered a pair of coupled pseudo-bimolecular reactions,⁶⁶ the overall difference in hydrogen bond

1 potential well depth is determined by the difference in pK_a values between the two protonated states,
2 ΔpK_a .⁶⁷ These concepts are readily translatable to the consideration of proton exchange dynamics at solid-
3 liquid interfaces. Crucially, for the purpose of rationalising the observed trend between relaxation
4 characteristics and adsorbate pK_a detailed in **Figure 4b**, we recognise that for the comparison of exchange
5 processes between a single silica material and multiple distinct adsorbates, changes in ΔpK_a may be assumed
6 dependent on only the adsorbate pK_a . With the free energy minimum associated with the solid surface
7 essentially fixed across the range of experiments performed, adsorbate pK_a will therefore indirectly dictate
8 the free energy barrier height, in turn influencing observable proton exchange rates $k = k_1 + k_2$. We
9 therefore consider adsorbate pK_a an approximate and indirect indicator of overall hydroxyl group exchange
10 rates, in turn providing a generalised rationale for the correlation observed in **Figure 4b**. This reasoning is
11 further consistent with the peak integral ratio data presented in **Figure 3**, wherein the observed alkyl/hydroxyl
12 ratios of our adsorbates are clearly reduced from their expected values in order of increasing acidity;
13 adsorbates undergoing significant surface-adsorbate proton exchange will present larger hydroxyl relaxation
14 populations than expected, hence reducing the experimentally observed alkyl/hydroxyl ratio.

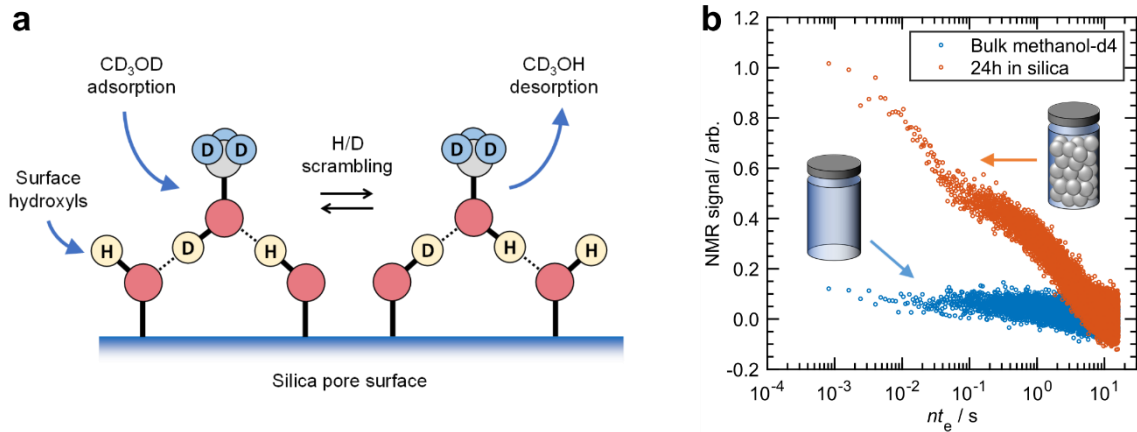
15 To support the above interpretation, the ability of our model silica material to undergo proton exchange
16 interactions with adsorbed hydrocarbons was confirmed via deuterium exchange experiments, with
17 methanol-d4 (CD_3OD ; $D \equiv {}^2H$) utilised as a probe fluid. The salient features of the expected solid-liquid
18 interactions are shown in **Figure 5a**. In the absence of interfacial proton exchange the methanol-d4 probe will
19 remain invisible to 1H NMR analysis; if exchange occurs, however, we expect a growth in detectable 1H NMR
20 signal as surface proton scrambling facilitates the formation of CD_3OH . **Figure 5b** compares 1H T_2 decay data
21 from methanol-d4 (nominal purity = 99.8 %) with that from a sample of mesoporous silica exposed to excess
22 methanol-d4 for 24 hours; unlike the samples prepared for 2D $T_1 - T_2$ analysis, this system therefore
23 comprises both free and confined liquid. While signal arising from the neat sample (bulk methanol-d4) lies
24 within the spectrometer noise floor, the system comprising mesoporous silica in excess methanol-d4 clearly
25 exhibits an observable T_2 decay signal, confirming the presence of NMR active CD_3OH , and hence the
26 occurrence of surface-adsorbate proton exchange interactions. **Supplementary Note 2** further explores the
27 consistent temporal increase of this detectable signal over the first 24 hours.



1

2 **Figure 4. Relaxation trends of protic adsorbates.** a Summary of modal alky and hydroxyl ^1H relaxation time
 3 ratios $\langle T_1/T_2 \rangle$; values correspond with the dashed diagonal lines in **Figure 2**. b Correlation between the
 4 difference in alkyl and hydroxyl relaxation time ratios $\Delta\langle T_1/T_2 \rangle$ and adsorbate pK_a , including a linear fit. c
 5 Double-well potential energy surface for proton exchange between hydrogen bond donors (D) and acceptors
 6 (A). The forward and back exchange rates k_1 and k_2 are hence determined by the activation free energies
 7 $\Delta^\ddagger G_1$ and $\Delta^\ddagger G_2$, respectively, while the difference in potential well depth is determined by the difference in
 8 pK_a of the two protonated states, ΔpK_a .

9



1

2 **Figure 5. Proton scrambling at the methanol/silica interface.** a Expected interactions between methanol-d4
 3 (CD₃OD) and silica pore surfaces. ¹H NMR-invisible CD₃OD molecules adsorb via hydrogen bonding interactions
 4 with surface hydroxyl groups, facilitating H/D scrambling. Desorbing CD₃OH will then be visible to ¹H NMR
 5 analysis. b CPMG T_2 decay data for bulk CD₃OD (blue) and CD₃OD combined in excess with dry mesoporous
 6 silica for 24 hours (orange). The clear ¹H T_2 decay signal in the case of CD₃OD imbibition within silica confirms
 7 surface H/D scrambling and the formation of ¹H NMR-active CD₃OH.

1 **Conclusions**

2 The identification of functional group-specific nuclear spin relaxation across the diverse range of adsorbates
3 examined here is of clear significance for the accurate interpretation of NMR relaxation data acquired from
4 systems involving polar-protic probe fluids and hydroxylated pore surfaces. The example solid/liquid systems
5 explored here are of particular relevance to the interrogation of solvent effects in liquid-phase heterogeneous
6 catalysis, wherein the utilisation of nuclear spin relaxation measurements to infer interfacial phenomena is
7 now a rapidly evolving field. Furthermore, the unambiguous assignment of multiple relaxation populations to
8 individual adsorbates undergoing surface-adsorbate proton exchange is expected to better inform the
9 application and interpretation of multidimensional relaxation measurements when applied to a range of
10 complex porous systems, averting the erroneous interpretation of correlation data in terms of material
11 structures or the presence of multiple adsorbates. Although not explored here, we note that the clear
12 distinction between alkyl and hydroxyl relaxation populations along the T_2 dimension of our 2D correlation
13 data suggests functional group-specific insight is also readily accessible via rapid one-dimensional T_2
14 measurements, facilitating the extension of such analyses to temporally resolved experimental systems; this
15 concept is of particular relevance to the study of competitive displacement dynamics, which we aim to pursue
16 in future work. Finally, we note that the clear correlation between nuclear spin relaxation characteristics and
17 adsorbate acidity strongly motivates further investigation into how relaxation phenomena may be exploited
18 as a robust and non-invasive probe of adsorbate identity and/or material surface chemistry within a diverse
19 range of porous architectures.

20

21

1 **Methods**

2 **Materials and sample preparation**

3 A commercial Q15 mesoporous silica gel material (4 mm diameter spherical particles; nominal mean pore size:
4 15 nm) was obtained from Fuji Silysia Chemical Ltd. (Japan). The material was first refluxed in deionised water
5 (obtained onsite at the Australian Resources Research Centre, Perth, Australia) at 120 °C for 4 hours to
6 hydroxylate the pore surfaces. The Q15 was then dried in air at 110 °C for 12 hours, and for an additional 3
7 hours at 110 °C under vacuum (10^{-3} bar).

8 Cyclohexane (Thermofisher Scientific, >99%), acetone (ChemSupply Australia, >98%), methanol (ChemSupply
9 Australia, >99.9%), ethanol (ChemSupply Australia, >99.9%), 1-propanol (ChemSupply Australia, >99.8%), 2-
10 propanol (ChemSupply Australia, >99.5%), 1-butanol (ChemSupply Australia, >99%), 2-butanol (ChemSupply
11 Australia, >99%), acetic acid (Merk, >99%), propanoic acid (ChemSupply Australia, >99%), butanoic acid
12 (ChemSupply Australia, >99%), and methanol-d4 (Cambridge Isotope Laboratories, 99.8%) were used as
13 received.

14 Imbided silica samples for $T_1 - T_2$ analysis were prepared by soaking in excess liquid for at least 48 hours
15 under ambient conditions. Silica particles were then separated from each liquid and rolled over a pre-soaked
16 filter paper to remove any inter-particle liquid, with the imbided silica spheres transferred to sealed 7 ml glass
17 vials for analysis. Each sample consisted of approximately 2.5 g of Q15, corresponding with around 160
18 particles; as such, each sample provided a well-averaged measurement of the surface-adsorbate interactions
19 present between probe liquid and the model silica material employed. Sample preparation for methanol-d4
20 exchange analysis is described in **Supplementary Note 2**.

21 **NMR hardware**

22 ^1H nuclear spin relaxation measurements were performed using an Oxford Instruments Geospec NMR
23 spectrometer equipped with a $B_0 = 0.3$ T parallel plate permanent magnet array (providing a ^1H frequency of
24 $\nu_0 = 12.7$ MHz) and a 53 mm Q-sense probe. All measurements were performed at room temperature ($25 \pm$
25 1 °C) and ambient pressure.

26 **2D relaxation analysis**

27 $T_1 - T_2$ relaxation correlation data was acquired by applying the 2D pulse sequence in **Figure 1a**,²⁰ wherein
28 90° and 180° radio frequency (RF) pulses are represented by thin and thick vertical bars, respectively.
29 Following initial polarisation of the spin system along the direction of the static magnetic field B_0
30 (conventionally termed the z-axis), a 180° RF pulse inverts the sample magnetisation onto the -z axis. Here,
31 longitudinal T_1 relaxation processes drive the spin system back towards thermal equilibrium; this recovery is

1 characterised by the relaxation time constant T_1 , and was encoded within the indirect dimension of our 2D
 2 relaxation data through the application of a variable recovery time τ . The spin system is then rotated into the
 3 transverse plane via a 90° RF pulse, inducing transverse relaxation processes. A train of n 180° RF pulses
 4 induces n spin echoes, which decay in magnitude due to T_2 ; each echo magnitude $S(nt_e, \tau)$ was recorded as
 5 a single data point (white data point in **Figure 1a**), defining the direct dimension of our relaxation data. The
 6 pulse sequence was then cycled to encode for m different τ recovery times, forming an $(m \times n)$ data surface
 7 (**Figure 1d**). The indirect dimension of our measurements was encoded by employing 16 logarithmically spaced
 8 τ values between 1 ms and 12 s, while the direct dimension was encoded using $n = 40,000$ echoes separated
 9 by an echo time of $t_e = 100 \mu\text{s}$. This short echo time, together with the low static magnetic field strength used
 10 here, was employed to mitigate undesired transverse relaxation phenomena resulting from magnetic
 11 susceptibility contrast effects at the solid-liquid interface.³⁵ Measurements included 8 repeat scans separated
 12 by a recycle delay of 12 s ($\gg 5 \times T_1$), taking approximately 40 minutes per correlation measurement and
 13 resulting in signal-to-noise ratios of approximately 400.

14 $T_1 - T_2$ relaxation correlation data may be described by a 2D Fredholm integral equation of the first kind:⁴⁷

$$\frac{S(nt_e, \tau)}{S(0, \infty)} = \iint K_{12}(nt_e, T_2, \tau, T_1) F(T_1, T_2) d \log_{10}(T_1) d \log_{10}(T_2) + \varepsilon(nt_e, \tau). \quad (4)$$

15 Here $S(nt_e)/S(0, \infty)$ is the normalised spin echo signal magnitude, while $\varepsilon(nt_e, \tau)$ represents the
 16 experimental noise, assumed Gaussian with zero mean. The kernel function $K_{12}(nt_e, T_2, \tau, T_1)$ describes the
 17 predicted form of T_1 and T_2 relaxation, which for the pulse sequence in **Figure 1a** is given by:²⁰

$$K_{12}(nt_e, T_2, \tau, T_1) = \left[1 - 2 \exp\left(\frac{-\tau}{T_1}\right) \right] \exp\left(\frac{-nt_e}{T_2}\right). \quad (5)$$

18 Finally, the term $F(T_1, T_2)$ represents the targeted 2D distribution of T_1 and T_2 relaxation time constants.
 19 Distributions were obtained via a numerical inversion of each acquired relaxation data surface according to
 20 Equations (4) and (5). As this is an ill-posed problem in the presence of experimental noise,⁴¹ stability of the
 21 inverted distributions was achieved through the application of Tikhonov regularisation,⁶⁸ with the degree of
 22 smoothing determined via the generalised cross-validation (GCV) method.⁶⁹ Distributions were limited to
 23 (200×200) values, with each dimension bound within the range $\{10^{-4}, 10^1\}$ s (note that correlation plots in
 24 **Figure 1** are shown with reduced bounds to increase correlation peak clarity). Inversions were performed using
 25 a 2D fast Laplace inversion algorithm written in Matlab, as first implemented by Mitchell *et al.*⁷⁰

26 H/D exchange

27 For the analysis of H/D exchange at the methanol-d4/silica interface, T_2 decay data was acquired by applying
 28 the standard Carr-Purcell Meiboom-Gill (CPMG) sequence. The magnitude of $n = 40,000$ spin echoes were
 29 acquired separated by an echo time of $t_e = 400 \mu\text{s}$. Further details are provided in **Supplementary Note 2**.

1 **Acknowledgements**

2 The authors thank Fuji Silysia (Japan) for providing the mesoporous silica and acknowledge funding from the
3 Australia Research Council (IC150100019 and LP1801001116).

4

5 **Additional information**

6 **Author Contributions**

7 N.R. and M.L.J. designed the research. N.R. performed the experiments and analysed the data. E.F.M and
8 M.L.J. supervised the research. N.R. and M.L.J wrote the manuscript. All authors discussed the results and
9 commented on the manuscript.

10 **Supplementary Information Details**

11 The Supplementary Information file contains:

- 12 • Supplementary Note 1: Surface Relaxation Theory
- 13 • Supplementary Note 2: Methanol-d4 Exchange Experiments
- 14 • Supplementary Table 1
- 15 • Supplementary Figures 1 – 3

16 **Data Availability**

17 Associated data is available in the Supplementary Information file or from the corresponding author upon
18 reasonable request.

19 **Competing Interests**

20 The authors declare no competing interests.

1 References

- 2 1. Zaera, F. Surface chemistry at the liquid/solid interface. *Surface Science* **605**, 1141–1145 (2011).
- 3 2. Zaera, F. Probing liquid/solid interfaces at the molecular level. *Chem. Rev.* **112**, 2920–2986 (2012).
- 4 3. Gladden, L. F. & Mitchell, J. Measuring adsorption, diffusion and flow in chemical engineering:
5 applications of magnetic resonance to porous media. *New J. Phys.* **13**, 035001 (2011).
- 6 4. Kinn, B. E., Myers, T. R. & Allgeier, A. M. Surface enhanced nuclear magnetic resonance relaxation
7 mechanisms and their significance in chemical engineering applications. *Curr. Opin. Chem. Eng.* **24**,
8 115–121 (2019).
- 9 5. Kowalewski, J. & Mäler, L. *Nuclear spin relaxation in liquids: theory, experiments, and applications*. (CRC
10 Press, 2017).
- 11 6. Korb, J.-P. Multiscale nuclear magnetic relaxation dispersion of complex liquids in bulk and
12 confinement. *Prog. Nucl. Magn. Reson. Spectrosc.* **104**, 12–55 (2018).
- 13 7. Brown, R. J. S. The Earth's-field NMR development at Chevron. *Concepts Magn. Reson.* **13**, 344–366
14 (2001).
- 15 8. Kleinberg, R. L. NMR well logging at Schlumberger. *Concepts Magn. Reson.* **13**, 396–403 (2001).
- 16 9. Mitchell, J. & Fordham, E. J. Contributed Review: Nuclear magnetic resonance core analysis at 0.3 T.
17 *Rev. Sci. Instrum.* **85**, 111502 (2014).
- 18 10. Korb, J. P. NMR and nuclear spin relaxation of cement and concrete materials. *Current Opinion in Colloid
19 and Interface Science* **14**, 192–202 (2009).
- 20 11. Korb, J.-P. Nuclear magnetic relaxation of liquids in porous media. *New J. Phys.* **13**, 035016 (2011).
- 21 12. D'Agostino, C. *et al.* Solvent inhibition in the liquid-phase catalytic oxidation of 1,4-butanediol:
22 understanding the catalyst behaviour from NMR relaxation time measurements. *Catal. Sci. Technol.* **6**,
23 7896–7901 (2016).
- 24 13. Isaacs, M. A. *et al.* A spatially orthogonal hierarchically porous acid–base catalyst for cascade and
25 antagonistic reactions. *Nat. Catal.* **3**, 921–931 (2020).
- 26 14. Filippini, G. *et al.* Light-driven, heterogeneous organocatalysts for C-C bond formation toward valuable
27 perfluoroalkylated intermediates. *Sci. Adv.* **6**, 9923–9934 (2020).
- 28 15. Robinson, N. *et al.* Low-field NMR relaxation-exchange measurements for the study of gas admission
29 in microporous solids. *Phys. Chem. Chem. Phys.* **22**, 13689–13697 (2020).
- 30 16. Chen, J. J. *et al.* ExSitu NMR relaxometry of metal-organic frameworks for rapid surface-area screening.
31 *Angew. Chemie - Int. Ed.* **52**, 12043–12046 (2013).
- 32 17. Song, Y. Q. Magnetic resonance of porous media (MRPM): A perspective. *J. Magn. Reson.* **229**, 12–24
33 (2013).
- 34 18. Callaghan, P. T. *et al.* Recent Fourier and Laplace perspectives for multidimensional NMR in porous
35 media. *Magn. Reson. Imaging* **25**, 441–444 (2007).

- 1 19. Bernin, D. & Topgaard, D. NMR diffusion and relaxation correlation methods: New insights in
2 heterogeneous materials. *Curr. Opin. Colloid Interface Sci.* **18**, 166–172 (2013).
- 3 20. Song, Y.-Q. *et al.* T1–T2 Correlation Spectra Obtained Using a Fast Two-Dimensional Laplace Inversion.
4 *J. Magn. Reson.* **154**, 261–268 (2002).
- 5 21. Robinson, N., Robertson, C., Gladden, L. F., Jenkins, S. J. & D’Agostino, C. Direct correlation between
6 adsorption energetics and nuclear spin relaxation in a liquid-saturated catalyst material.
7 *ChemPhysChem* **19**, 2472–2479 (2018).
- 8 22. King, J. N., Lee, V. J., Ahola, S., Telkki, V. V. & Meldrum, T. Ultrafast Multidimensional Laplace NMR
9 Using a Single-Sided Magnet. *Angew. Chemie - Int. Ed.* **55**, 5040–5043 (2016).
- 10 23. Washburn, K. E. & Callaghan, P. T. Tracking Pore to Pore Exchange Using Relaxation Exchange
11 Spectroscopy. *Phys. Rev. Lett.* **97**, 175502 (2006).
- 12 24. Mitchell, J. *et al.* Validation of NMR relaxation exchange time measurements in porous media. *J. Chem.*
13 *Phys.* **127**, 234701 (2007).
- 14 25. Hürlimann, M. D. & Venkataramanan, L. Quantitative measurement of two-dimensional distribution
15 functions of diffusion and relaxation in grossly inhomogeneous fields. *J. Magn. Reson.* **157**, 31–42
16 (2002).
- 17 26. Hürlimann, M. D., Venkataramanan, L. & Flaum, C. The diffusion-spin relaxation time distribution
18 function as an experimental probe to characterize fluid mixtures in porous media. *J. Chem. Phys.* **117**,
19 10223–10232 (2002).
- 20 27. Ahola, S. *et al.* Ultrafast multidimensional Laplace NMR for a rapid and sensitive chemical analysis. *Nat.*
21 *Commun.* **6**, 1–7 (2015).
- 22 28. Mankinen, O. *et al.* Ultrafast diffusion exchange nuclear magnetic resonance. *Nat. Commun.* **11**, 1–8
23 (2020).
- 24 29. Sun, B. & Dunn, K. J. A global inversion method for multi-dimensional NMR logging. *J. Magn. Reson.*
25 **172**, 152–160 (2005).
- 26 30. Chandrasekera, T. C., Mitchell, J., Fordham, E. J., Gladden, L. F. & Johns, M. L. Rapid encoding of T1 with
27 spectral resolution in n-dimensional relaxation correlations. *J. Magn. Reson.* **194**, 156–161 (2008).
- 28 31. Arns, C. H., Washburn, K. & Callaghan, P. T. Multidimensional NMR inverse Laplace spectroscopy in
29 porous media. *Magn. Reson. Imaging* **25**, 548–549 (2007).
- 30 32. Zhang, Y., Xiao, L., Li, X. & Liao, G. T1–D–T2 correlation of porous media with compressed sensing at
31 low-field NMR. *Magn. Reson. Imaging* **56**, 174–180 (2019).
- 32 33. Terenzi, C., Sederman, A. J., Mantle, M. D. & Gladden, L. F. Spatially-resolved ¹H NMR relaxation-
33 exchange measurements in heterogeneous media. *J. Magn. Reson.* **299**, 101–108 (2019).
- 34 34. Vashae, S. *et al.* Local T1-T2 distribution measurements in porous media. *J. Magn. Reson.* **287**, 113–
35 122 (2018).
- 36 35. Mitchell, J., Chandrasekera, T. C., Johns, M. L., Gladden, L. F. & Fordham, E. J. Nuclear magnetic
37 resonance relaxation and diffusion in the presence of internal gradients: The effect of magnetic field

- 1 strength. *Phys. Rev. E* **81**, (2010).
- 2 36. Terenzi, C., Sederman, A. J., Mantle, M. D. & Gladden, L. F. Enabling High Spectral Resolution of Liquid
3 Mixtures in Porous Media by Antidiagonal Projections of Two-Dimensional ¹H NMR COSY Spectra. *J.*
4 *Phys. Chem. Lett.* **10**, 5781–5785 (2019).
- 5 37. Fleury, M. & Romero-Sarmiento, M. Characterization of shales using T1-T2 NMR maps. *J. Pet. Sci. Eng.*
6 **137**, 55–62 (2016).
- 7 38. Song, Y.-Q. & Kausik, R. NMR application in unconventional shale reservoirs – A new porous media
8 research frontier. *Prog. Nucl. Magn. Reson. Spectrosc.* **112–113**, 17–33 (2019).
- 9 39. Weber, D., Mitchell, J., Mcgregor, J. & Gladden, L. F. Comparing strengths of surface interactions for
10 reactants and solvents in porous catalysts using Two-dimensional NMR relaxation correlations. *J. Phys.*
11 *Chem. C* **113**, 6610–6615 (2009).
- 12 40. Thomas, J. M. & Thomas, W. J. *Principles and practice of heterogeneous catalysis. Principles and*
13 *practice of heterogeneous catalysis* (Wiley-VCH, 2015).
- 14 41. Mitchell, J., Chandrasekera, T. C. & Gladden, L. F. Numerical estimation of relaxation and diffusion
15 distributions in two dimensions. *Prog. Nucl. Magn. Reson. Spectrosc.* **62**, 34–50 (2012).
- 16 42. Brownstein, K. R. & Tarr, C. E. Importance of classical diffusion in NMR studies of water in biological
17 cells. *Phys. Rev. A* **19**, 2446–2453 (1979).
- 18 43. Barrie, P. J. Characterization of porous media using NMR methods. *Annual Reports on NMR*
19 *Spectroscopy* **41**, 265–316 (2000).
- 20 44. Mitchell, J., Broche, L. M., Chandrasekera, T. C., Lurie, D. J. & Gladden, L. F. Exploring Surface
21 Interactions in Catalysts Using Low-Field Nuclear Magnetic Resonance. *J. Phys. Chem. C* **117**, 17699–
22 17706 (2013).
- 23 45. Godefroy, S., Korb, J.-P., Fleury, M. & Bryant, R. G. Surface nuclear magnetic relaxation and dynamics
24 of water and oil in macroporous media. *Phys. Rev. E* **64**, 021605 (2001).
- 25 46. D’Agostino, C., Mitchell, J., Mantle, M. D. & Gladden, L. F. Interpretation of NMR Relaxation as a Tool
26 for Characterising the Adsorption Strength of Liquids inside Porous Materials. *Chem. - A Eur. J.* **20**,
27 13009–13015 (2014).
- 28 47. Venkataramanan, L., Yi-Qiao Song & Hurlimann, M. D. Solving Fredholm integrals of the first kind with
29 tensor product structure in 2 and 2.5 dimensions. *IEEE Trans. Signal Process.* **50**, 1017–1026 (2002).
- 30 48. Stapf, S., Kimmich, R. & Seitter, R. O. Proton and deuteron field-cycling NMR relaxometry of liquids in
31 porous glasses: Evidence for Lévy-walk statistics. *Phys. Rev. Lett.* **75**, 2855–2858 (1995).
- 32 49. D’Agostino, C., Mitchell, J., Gladden, L. F. & Mantle, M. D. Hydrogen Bonding Network Disruption in
33 Mesoporous Catalyst Supports Probed by PFG-NMR Diffusometry and NMR Relaxometry. *J. Phys.*
34 *Chem. C* **116**, 8975–8982 (2012).
- 35 50. Rottreau, T. J., Parlett, C. M. A., Lee, A. F. & Evans, R. Diffusion NMR Characterization of Catalytic Silica
36 Supports: A Tortuous Path. *J. Phys. Chem. C* **121**, 16250–16256 (2017).
- 37 51. Robinson, N. & D’Agostino, C. NMR Investigation into the Influence of Surface Interactions on Liquid

- 1 Diffusion in a Mesoporous Catalyst Support. *Top. Catal.* **63**, 319–327 (2020).
- 2 52. Aguilar, J. A., Nilsson, M., Bodenhausen, G. & Morris, G. A. Spin echo NMR spectra without J
3 modulation. *Chem. Commun.* **48**, 811–813 (2012).
- 4 53. Robinson, N., Gladden, L. F. & D’Agostino, C. Exploring catalyst passivation with NMR relaxation.
5 *Faraday Discuss.* **204**, 439–452 (2017).
- 6 54. Ward-Williams, J., Korb, J. P. & Gladden, L. F. Insights into Functionality-Specific Adsorption Dynamics
7 and Stable Reaction Intermediates Using Fast Field Cycling NMR. *J. Phys. Chem. C* **122**, 20271–20278
8 (2018).
- 9 55. Ward-Williams, J. *et al.* Characterizing Solid–Liquid Interactions in a Mesoporous Catalyst Support
10 Using Variable-Temperature Fast Field Cycling NMR. *J. Phys. Chem. C* **125**, 8767–8778 (2021).
- 11 56. D’Agostino, C., Chansai, S., Gladden, L. F. & Hardacre, C. Correlating the strength of reducing agent
12 adsorption with Ag/Al₂O₃ catalyst performances in selective catalytic reduction (SCR) of NO_x. *Catal.*
13 *Today* (2021). doi:10.1016/j.cattod.2021.01.013
- 14 57. Roy, D. *et al.* Nonpolar adsorption at the silica/methanol interface: Surface mediated polarity and
15 solvent density across a strongly associating solid/liquid boundary. *J. Phys. Chem. C* **117**, 27052–27061
16 (2013).
- 17 58. Han, J. W., James, J. N. & Sholl, D. S. First principles calculations of methylamine and methanol
18 adsorption on hydroxylated quartz (0 0 0 1). *Surf. Sci.* **602**, 2478–2485 (2008).
- 19 59. Ishikita, H. & Saito, K. Proton transfer reactions and hydrogen-bond networks in protein environments.
20 *J. R. Soc. Interface* **11**, 20130518 (2014).
- 21 60. Lowe, B. M., Skylaris, C. K. & Green, N. G. Acid-base dissociation mechanisms and energetics at the
22 silica-water interface: An activationless process. *J. Colloid Interface Sci.* **451**, 231–244 (2015).
- 23 61. Olivieri, G., Goel, A. & Brown, M. A. Molecular level insight on the adsorption of carboxylic acids to
24 oxide nanoparticles in aqueous solution by X-ray photoelectron spectroscopy. *Chem. Commun.* **52**,
25 9040–9043 (2016).
- 26 62. McDonald, P. J., Korb, J.-P., Mitchell, J. & Monteilhet, L. Surface relaxation and chemical exchange in
27 hydrating cement pastes: A two-dimensional NMR relaxation study. *Phys. Rev. E* **72**, 011409 (2005).
- 28 63. Kimmich, R. *Principles of soft-matter dynamics: Basic theories, non-invasive methods, mesoscopic*
29 *aspects. Principles of Soft-Matter Dynamics: Basic Theories, Non-invasive Methods, Mesoscopic Aspects*
30 (Springer Netherlands, 2012). doi:10.1007/978-94-007-5536-9
- 31 64. Van Landeghem, M., Haber, A., D’espinoise De Lacaillerie, J.-B. & Blümich, B. Analysis of multisite 2D
32 relaxation exchange NMR. *Concepts Magn. Reson. Part A* **36A**, 153–169 (2010).
- 33 65. Krzyżak, A. T. & Habina, I. Low field ¹H NMR characterization of mesoporous silica MCM-41 and SBA-
34 15 filled with different amount of water. *Microporous Mesoporous Mater.* **231**, 230–239 (2016).
- 35 66. Gilli, P., Bertolasi, V., Pretto, L. & Gilli, G. Outline of a transition-state hydrogen-bond theory. *J. Mol.*
36 *Struct.* **790**, 40–49 (2006).
- 37 67. Gilli, P., Pretto, L., Bertolasi, V. & Gilli, G. Predicting Hydrogen-Bond strengths from Acid-Base molecular

- 1 properties. the pKa slide rule: Toward the solution of a Long-Lasting problem. *Acc. Chem. Res.* **42**, 33–
2 44 (2009).
- 3 68. Tikhonov, A. N. & Arsenin, V. I. A. *Solutions of ill-posed problems*. (SIAM, 1977).
- 4 69. Golub, G. H., Heath, M. & Wahba, G. Generalized cross-validation as a method for choosing a good
5 ridge parameter. *Technometrics* **21**, 215–223 (1979).
- 6 70. Mitchell, J. *et al.* Determining NMR flow propagator moments in porous rocks without the influence of
7 relaxation. *J. Magn. Reson.* **193**, 218–225 (2008).

8